Rock Mechanics and Rock Engineering
https://doi.org/10.1007/s00603-026-05805-4

ORIGINAL PAPER

RoDiAn: A Tool for Kinematic and Dynamic Stability Analysis of Discrete Blocks in Masonry and Engineered Rock Structures

Eugenio Segabinazzi[1] · Teresa Salvatici[1] · Giovanni Gigli[1] · Adrián J. Riquelme[2] · Emanuele Intrieri[1]

Received: 9 February 2026 / Accepted: 7 July 2026

Abstract
Historic masonry buildings and engineered rock structures characterized by discrete block assemblies are susceptible to gravitational failures along pre-existing geological discontinuities within individual blocks, similarly to rockfall phenomena occurring in natural settings. Conventional rock slope stability workflows and software, developed for large-scale natural formations, are incompatible with the specific geometric and spatial needs of this application. This paper presents RoDiAn (Rock Discontinuity Analyzer), a MATLAB application that addresses these limitations through the analysis of 3D point clouds (3DPC). RoDiAn implements novel algorithms for validating whether plane intersections form wedges within block geometry, determining discontinuity-retaining underlying structure (e.g., a facade) interactions, calculating kinematic susceptibility indices adapted from the slope mass rating system, and computing safety factors through limit equilibrium analysis with automated volume and contact area determination. Validation against synthetic geometries and real-world data demonstrates computational accuracy; kinematic analysis shows complete agreement with industry-standard software with added spatial filtering capabilities. Application to sandstone blocks from an historical palace in Florence (Italy) successfully identifies multiple failure mechanisms with quantified resisting and driving forces. RoDiAn provides heritage conservation professionals and geoscientists with an accessible quantitative methodology based on free software complete of a graphical user interface.

Highlights

- RoDiAn is a tool developed for the kinematic and dynamic stability analysis of rock blocks in masonry and engineered rock structures.
- A new methodological framework for quantifying rockfall susceptibility in discrete blocks is proposed.
- The method is 3D point-cloud based and uses data from LiDAR or photogrammetry.
- The tool is implemented as a MATLAB application with a graphical user interface designed for geoscientists and heritage conservation professionals.

Keywords Rock discontinuity · Kinematic analysis · Dynamic analysis · 3D point cloud processing · Cultural heritage

1 Introduction

Rockfall is a common hazard in mountainous terrains and steep rock slopes, typically triggered by the detachment of rock blocks along pre-existing joints and discontinuities (Dorren 2003). While rockfall phenomena are often studied in natural environments (Hantz et al. 2021, Chang et al. 2024), and in engineering and mining applications (Wang et al. 2024), similar hazards can emerge in the context of masonry buildings (Segabinazzi et al. 2024). Many structures, particularly those constructed from natural stone

✉ Eugenio Segabinazzi
eugenio.segabinazzi@unifi.it

[1] Department of Earth Sciences, University of Florence, Via Giorgio La Pira, 4, 50121 Florence, Italy

[2] Departamento de Ingeniería Civil, Universidad de Alicante, Alicante, Spain

Published online: 24 July 2026

blocks, are subject to rockfall-like failures due to weathering, structural decay, and jointing in the blocks (Salvatici et al. 2023). These processes can lead to the detachment of portions of stone blocks from building facades or rock engineered structures, resembling the natural slope failures observed in geological settings. In urban contexts where historical masonry extensively uses natural stone, such as in Florence, Italy, numerous incidents of detachment of stone elements from heritage facades have been reported in recent years (a survey from 1977 to 2009 (Gurrieri 2009) recorded more than 50 gravitational failures across 32 sites) including a tragic fatality at the Basilica of Santa Croce in 2017 (Segabinazzi et al. 2026) Warning signs about falling rock fragments have since been posted outside Palazzo Pitti, an emblematic acknowledgment that the problem is recognized. Despite these hazards, conventional conservation practices do not employ systematic methods for evaluating detachment risk or prioritizing interventions across building facades. Developing such systematic methods necessitates fundamental understanding of the underlying failure mechanisms: the morphological characteristics of gravitational failures observed in natural stone elements consistently demonstrate activation along pre-existing geological discontinuities, with detachment surfaces exhibiting fresh rock exposure that clearly indicates separation along natural weakness planes. Field observations conducted during this research have documented numerous examples of these failure mechanisms across various architectural elements. These events range in scale from small-scale spalling of individual laminations, producing fragments of a few hundred grams, to large-scale detachment of substantial block portions exceeding several kilograms (Palamidessi et al. 2026). The consistency of these patterns suggests that gravitational failure mechanisms represent systematic rather than random processes, governed by predictable geometric relationships that occur similarly to what is observed in rockfall phenomena on natural slopes (Fig. 1).

Numerical methods such as the discrete element method (DEM), implemented in codes including UDEC and 3DEC (Itasca, 2019, 2023), and the finite element method (FEM) are routinely applied to masonry structural analysis in heritage contexts and solve global structural behavior and multi-block interaction (Schiavoni et al. 2024). However, the failure mechanisms investigated in the present study (gravitational sliding and free-fall detachment along pre-existing geological discontinuities within individual discrete blocks) are appropriately represented through rigid-block limit equilibrium analysis. For this reason, rigid-block modeling was adopted as the preferred approach to describe the geometrical stability of the blocks from a geological perspective, while not excluding the complementary use of numerical methods where appropriate. The direct application of limit equilibrium workflows developed for natural slopes (Pantelidis 2009; Azarafza et al. 2021; Jaiswal et al. 2024) to heritage structures, however, presents methodological incompatibilities.

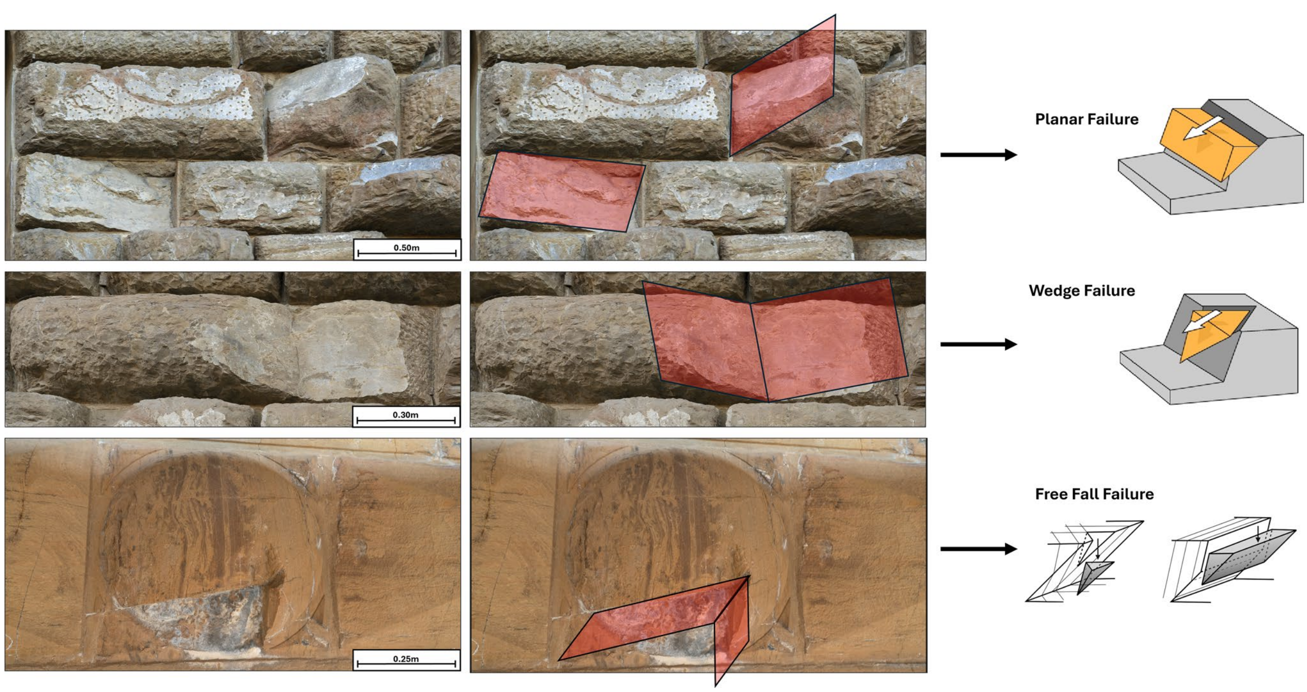

Fig. 1 Examples of gravitational failures in rock architectural elements, showing detachment along pre-existing geological discontinuities with fresh rock exposure on failure surfaces that can be assimilated to conventional rock failure modes

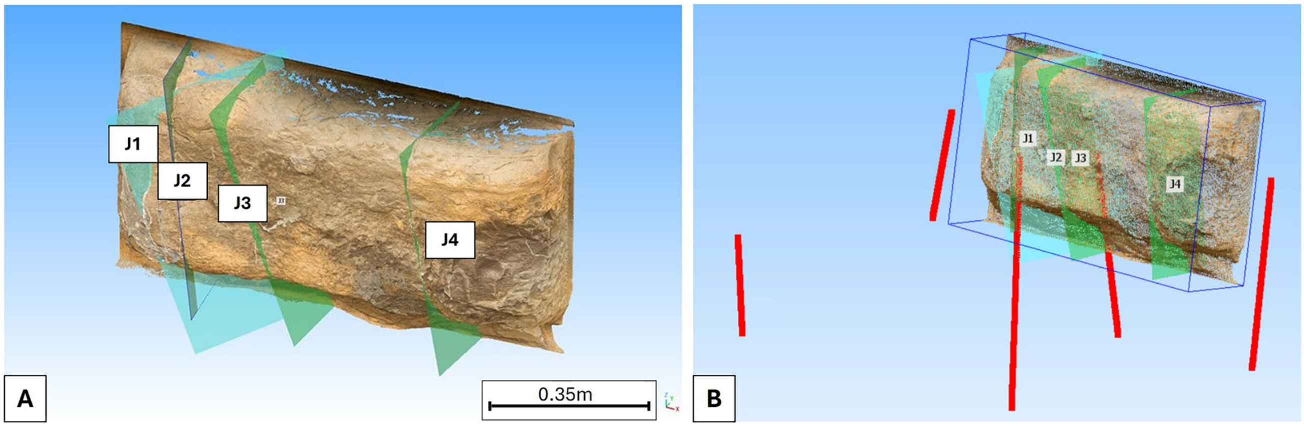

Fig. 2 **A:** Block that contains four discontinuity planes (J1-J2-J3-J4). Only the intersections between the planes 1–2 and 1–3 actually create wedges in the block (left). **B**: Visualization of the example block model showing all computed intersection lines between discontinuity planes, highlighted in red. As illustrated, several plane intersections extend beyond the block's geometry, occurring in spatial regions not relevant to the analysis

Commercial large-scale rock slope stability packages such as *RocScience Dips* and *Swedge* incorporate geometric assumptions developed for natural slope applications that cannot adequately represent the characteristics of discrete blocks in structures. Conventional slope stability software defines discontinuities solely through angular parameters (dip and dip direction), which describes families of parallel planes with assumed semi-infinite extension and without positional awareness. This approach operates on the premise that discontinuity families will inevitably intersect somewhere within the slope mass to form wedges. However, at the scale of individual discrete blocks in structures, typically measuring decimeters to a few meters, this assumption breaks down. Individual blocks contain discontinuities with limited trace lengths that may terminate within block boundaries, and plane intersections may not occur in spatial regions inside the actual element geometry (Fig. 2). Research-oriented software tools designed specifically for rock slopes, such as *DSE* (Riquelme et al. 2014), *Diana* (Gigli and Casagli 2011) and *Diana-K* (Gigli et al. 2022) share these fundamental limitations. Platforms that rely on the identification and characterization of discontinuity families, through statistical analysis of orientation data (*DSE*), presume the existence of naturally occurring, regionally extensive joint sets. In heritage structures, these features do not conform to the natural clustering patterns, as the blocks are modified in the quarrying and shaping process. The algorithms calibrated on slope geometry (*Diana, Diana-K*) tend to misclassify potentially unstable regions, since they rely on superficial features which, in this case, do not represent the actual drivers of instability.

While tools such as commercially available packages (*RocScience RocSlope2, RocSlope3*) and research-oriented platforms like *DICE* (Menegoni et al. 2023), *ROKA* (Menegoni et al. 2021) and the Compass plugin for *CloudCompare* (Thiele et al. 2017) often adopting the conventional Baecher disk model (Jiang et al. 2024) can work with individual discontinuities, none of them provides the combination of capabilities required for discrete architectural elements: (i) full 3D spatial positioning and geometric filtering of wedge intersections within block boundaries, (ii) a facade interaction test distinguishing sliding from free-fall mechanisms, (iii) an integrated kinematic-to-dynamic pipeline with automated volume and contact area derivation from the point cloud, and (iv) computation of residual driving forces for the design of restraint and fall-arrest devices.

This geometric and methodological incompatibility creates a critical gap, that can be solved with a tool capable of:

1. Defining the spatial position of individual discontinuity planes, not just their orientation.
2. Filtering the wedges by calculating whether planes intersections occur within the point cloud boundaries.
3. Calculating the spatial interactions between discontinuity planes and a plane that represents the retaining underlying structure (a facade in case of buildings, a cut face in case of engineered rock structures).
4. Computing the volume and area of the unstable elements of the point cloud needed for dynamic analysis.
5. Performing stability calculations using limit equilibrium analysis on single discrete point cloud sections.

This paper presents RoDiAn (Rock Discontinuity Analyzer) a custom software developed specifically to address these limitations.

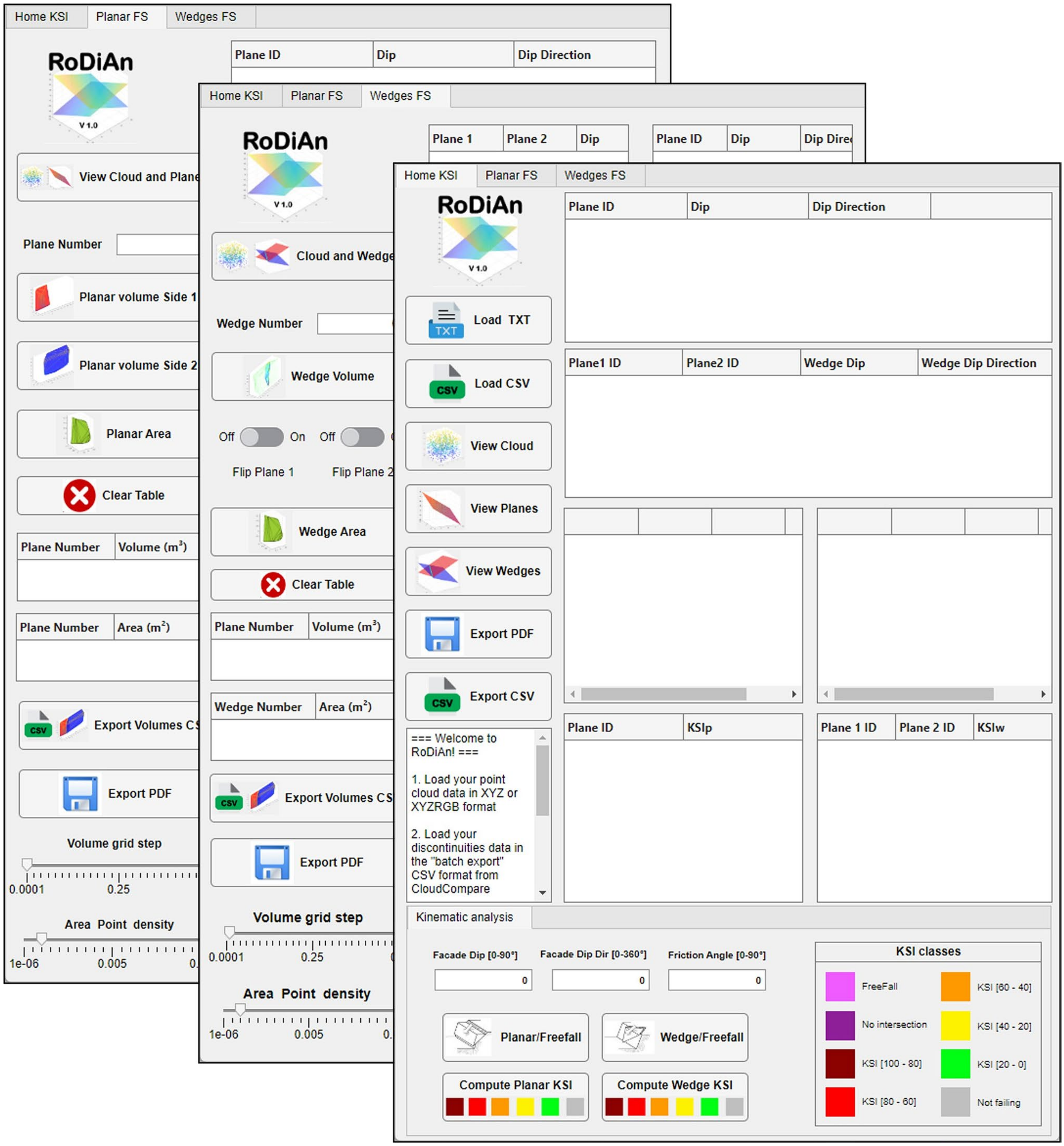

Fig. 3 RoDiAn graphical user interface showing the three primary analysis modules: Home KSI (Kinematic test and susceptibility assessment module), Planar FS (Dynamic analysis for planar sliding mechanisms), and Wedge FS (Dynamic analysis for wedge sliding mechanisms)

2 Software Architecture

2.1 Development Framework

RoDiAn is implemented as a MATLAB application, provided with a graphical user interface. The software is structured around three primary analysis modules organized as separate tabs (Fig. 3):

- Home KSI: Kinematic test and susceptibility assessment module

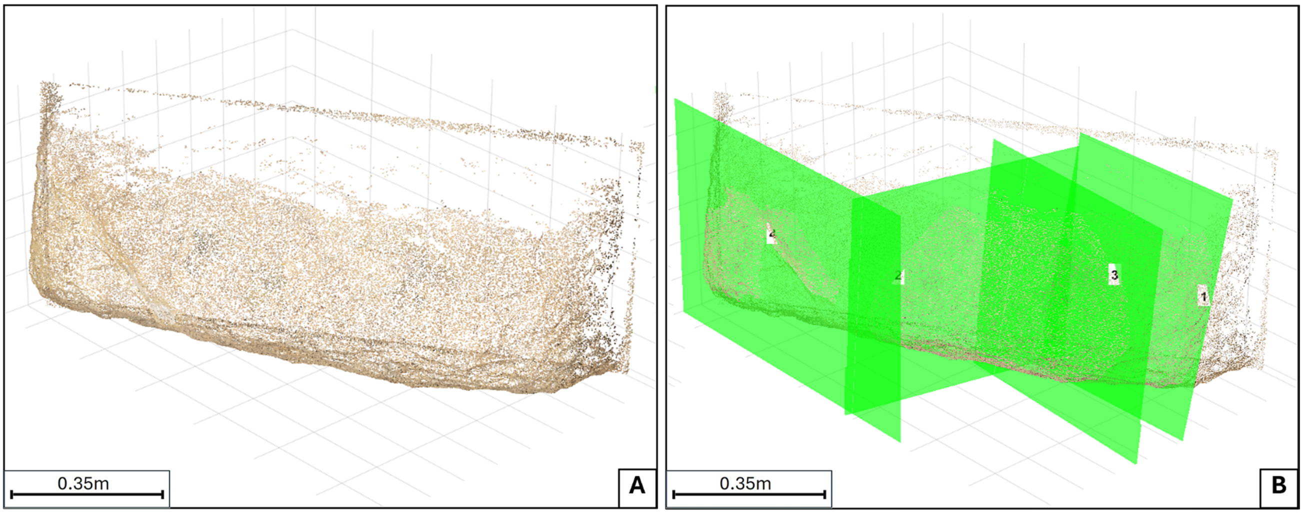

Fig. 4 Point cloud (**A**) and planes (**B**) visualization in RoDiAn

- Planar FS: Dynamic analysis for planar sliding mechanisms
- Wedge FS: Dynamic analysis for wedge sliding mechanisms

2.2 Input Data Structure

RoDiAn requires two input files:

1. A 3D point cloud (ascii format, XYZ or XYZRGB) representing the rock element.
2. A.csv file containing discontinuity plane information with both angular parameters and spatial coordinates.

The.csv file is generated from the 3D point cloud using a pre-processing workflow in the open-source software *CloudCompare:*

1. Import and trace: the 3D point cloud is imported into *CloudCompare*. The user traces points along the visible line of discontinuity using the 'Point List Picking' tool. This creates a new, separate point cloud composed only of the selected points. This process is repeated for each discontinuity being analyzed.
2. Fit Plane: by selecting one of the newly created "trace" point clouds, the user can fit a best-fit plane using the 'Fit—> Plane' tool.
3. Batch Export: after all discontinuity planes have been fitted, their data is exported at once using the 'Batch Export—> Export Plane Info' tool, which generates the required.csv file that is automatically read by RoDiAn.

3 Core Functionalities

3.1 Visualization and Data Validation

The initial functions enable users to load and visualize input data to verify correct file formatting and spatial registration (Fig. 4). The 'View Planes' function constructs planar surfaces in 3D space using the center point and normal vector extracted from the.csv data. To render these planes, the software:

1. Constructs an orthonormal basis lying within each plane through cross products with a reference vector.
2. Generates a 2D grid over the plane surface.
3. Clips the plane to the point cloud bounding box.
4. Labels each plane by its row index for subsequent analysis.

3.2 Wedge Identification and Spatial Filtering

The 'View Wedges' function addresses the fundamental problem of identifying which plane intersections actually form wedges within the block geometry. RoDiAn's calculates the intersections and their position with the following algorithm:

1. For each plane pair, compute the direction vector of their intersection line through the cross product of their normal vectors.
2. Solve the linear system defined by both plane equations to find a point on the intersection line.
3. Generate the full intersection line by projecting in both directions from this point.

4. Test whether any portion of the line falls within the block geometry using a convex hull representation of the point cloud.

Only intersections with portions inside the convex hull are retained as genuine wedges. For each validated wedge, the software calculates and stores the plunge and trend of the intersection line for subsequent kinematic analysis.

3.3 Kinematic Analysis

3.3.1 Geometric Feasibility Assessment

The kinematic analysis functions evaluate whether the geometric configuration of discontinuities permits gravitational failure.

The 'Planar/Freefall' function assesses each discontinuity plane against standard kinematic criteria for planar sliding (Markland test):

1. The discontinuity dip direction must fall within ± 20° of the facade or slope front dip direction.
2. The discontinuity dip angle must be less than the facade dip but greater than the friction angle.

The ± 20° angular tolerance applied to the dip direction alignment criterion is the standard value adopted as the conventional threshold in rock slope kinematic analysis (Hudson and Harrison 2007; Wyllie and Mah 2004). In the current implementation of RoDiAn, this tolerance is a fixed parameter and is not user-adjustable.

RoDiAn extends the analysis by also determining whether the plane intersects the retaining underlying structure (Fig. 5). This distinction is critical because planes that intersect the retaining structure benefit from additional cohesive restraint and structural support, whereas planes that do not intersect it represent fully isolated blocks with no such resistance, that is a more hazardous configuration. The software automatically creates a reference plane representing the retaining structure position based on point cloud geometry and user-specified orientation, then samples points across each discontinuity plane to test for intersection through the following algorithm:

1. Define the retaining structure orientation vectors using the input provided by the user (its dip and dip direction, already defined for the kinematic test).
2. Define the retaining structure position and dimensions by projecting all point cloud points onto the reference plane normal direction. It identifies the shallowest projection to locate the backside of the point cloud.
3. Transform the point cloud to plane coordinates by translating all points relative to the plane origin, then projecting them onto the plane internal basis vectors to obtain 2D coordinates within the reference plane.
4. Generate sample points on each discontinuity on a grid across the plane extent.
5. Test intersection for each sample point of the discontinuity by transforming point coordinates into the reference plane local coordinate system and verifying horizontal and vertical boundary compliance and the proximity to the surface within a threshold distance, marking the entire plane as intersecting if any sample point satisfies all criteria (Fig. 5).

The threshold distance used to determine whether a sample point is sufficiently close to the reference plane to qualify as intersecting is set by default to 5% of the maximum point cloud extent along the facade normal direction. The threshold becomes critical for planes whose sample points cluster very close to the facade boundary, in such borderline cases users are advised to visually verify the classification outcome using the 3D intersection visualization output. The planar facade approximation inherent to the reference plane definition performs well for regularly dressed stone facades. For blocks located at geometric transitions (corners, pillars, recesses) the reference plane orientation used in the facade interaction test should be set to represent the most relevant free face for that specific block rather than the overall facade orientation. Failure to do so may result in incorrect classification of the kinematic mechanism at boundary locations.

Four classification outcomes are possible:

- Kinematically stable configurations.
- Planar sliding with retaining structure contact.
- Planar sliding without retaining structure contact.
- Freefall scenarios.

The 'Wedge/Freefall' function applies analogous logic to wedge geometries, testing intersection lines against kinematic criteria and checking for retaining structure contact.

3.3.2 Kinematic Susceptibility Index

To move beyond binary classification (fail/no fail), RoDiAn calculates a Kinematic Susceptibility Index (KSI). This susceptibility index, adapted from Kundu et al. (Kundu et al. 2022), provides a more nuanced indication than the binary pass/fail result obtained through traditional kinematic testing. The index is derived from the unfavourability criteria of the Slope Mass Rating (SMR) system (Romana 1993) a widely accepted rock mass classification framework used globally with consistently successful results and endorsed by numerous researchers as an effective tool for assessing rock slope stability (Romana et al. 2015; Siddique 2024).

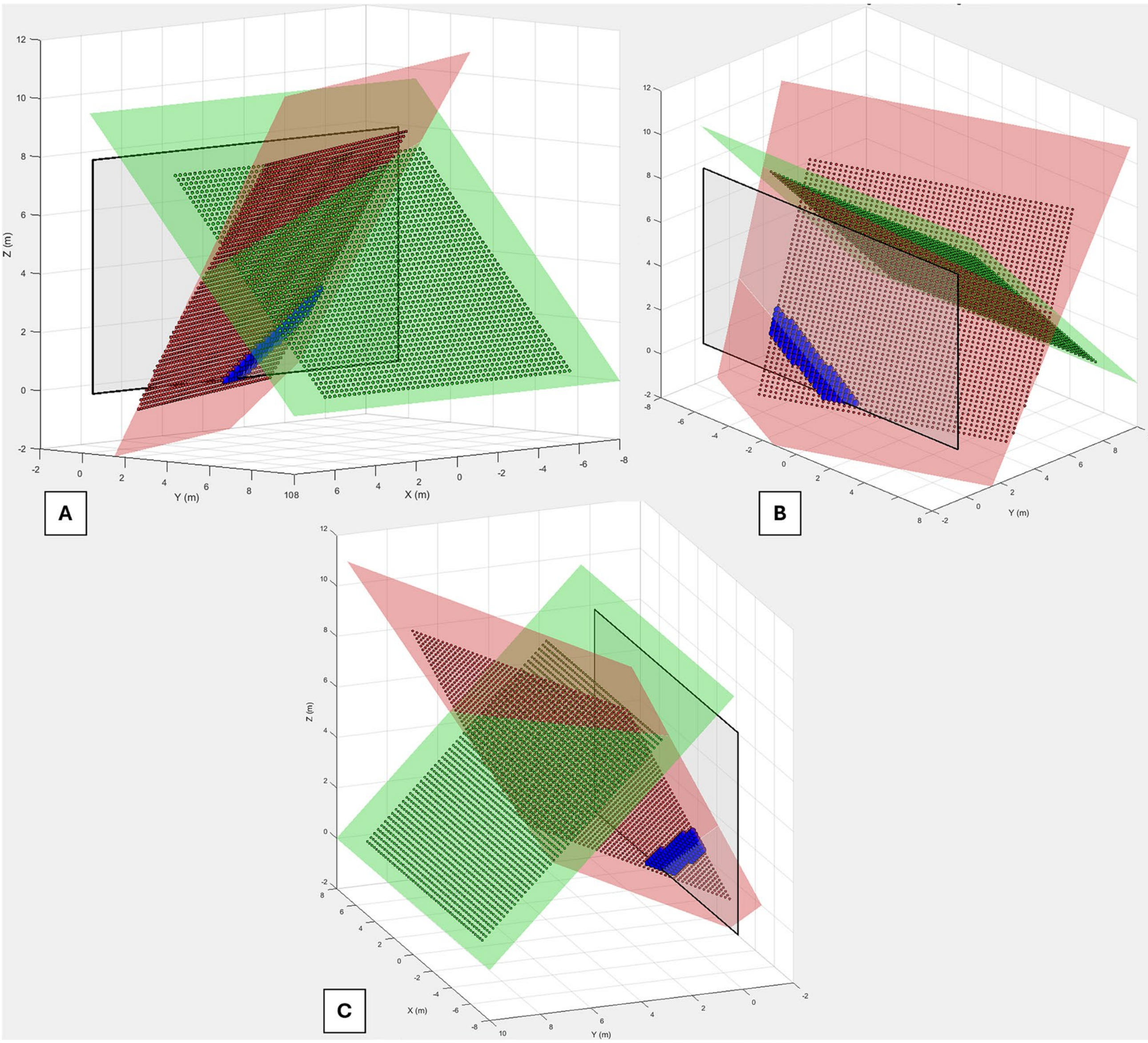

Fig. 5 Projection of sample points onto planes for intersection testing with the reference plane, 3D views from front left (**A**), back (**B**) and front right (**C**). A grid of points is generated on each plane and evaluated against the reference plane horizontal and vertical bounds. The facade is represented by the gray plane. The green plane does not intersect the reference plane, while the red plane does. Points confirming the intersection on the red plane are highlighted in blue

The KSI calculation employs the continuous functions developed by Tomás et al. (Tomás et al. 2007) for the SMR adjustment factors F1, F2, and F3, which have proven effective in evaluating the likelihood of unfavorable discontinuity configurations since their introduction. Factor F1 quantifies the degree of alignment between the discontinuity orientation and the slope face, with greater parallelism indicating higher failure susceptibility. It depends on angle A, which represents the angular relationship between discontinuity and slope orientations: for planar failure, this is the angle between the discontinuity dip direction and the slope dip direction, indicating parallelism between their strikes; for wedge failure, it is the angle between the azimuth of the intersection line and the dip direction of the slope. Factor F2 quantifies how the dip angle of the discontinuity influences the normal and shear stress distributions acting on the failure plane, with higher dip angles corresponding to greater susceptibility values. Factor F3 evaluates whether the geometric configuration allows the discontinuity to daylight (intersect and become visible) at the slope face, which is a prerequisite for kinematic instability. For planar failure, angle C is the difference between the discontinuity dip angle and the slope dip angle; for

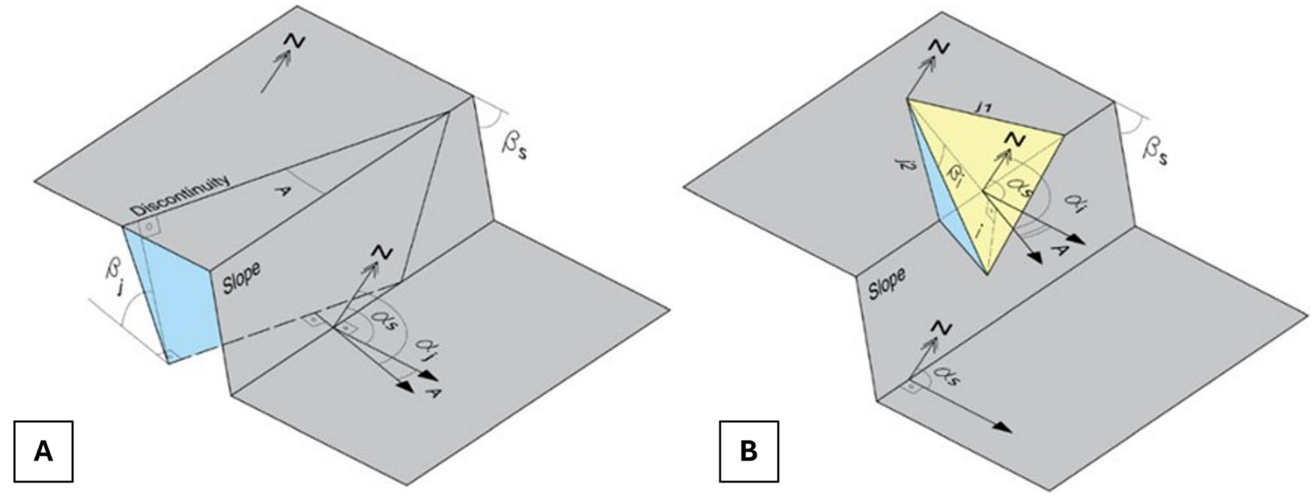

Fig. 6 **A:** Parallelism (angle A) between discontinuity and slope strikes for planar failure **B:** Parallelism (angle A) between the plunge direction of the line of intersection of two discontinuities (angle αi) and the slope dip direction (angle αs) for wedge failure (Adapted from Pastor et al. (2019))

wedge failure, it is the difference between the plunge of the intersection line and the slope dip angle (Fig. 6).

The mathematical formulations of these factors are:

$$F_1 = \frac{16}{25} - \frac{3}{500}\tan^{-1}\left(\frac{1}{10}(|A| - 17)\right) \quad (1)$$

$$F_2 = \frac{9}{16} + \frac{1}{195}\tan^{-1}\left(\frac{17}{100}B - 5\right) \quad (2)$$

$$F_3 = -30 + \frac{1}{3}\tan^{-1}(C) \quad (3)$$

The product of factors F1, F2, and F3 yields a value ranging from 0 (minimum susceptibility) to − 60 (maximum susceptibility). This range is normalized to a 0–100 scale using the expression:

$$Susceptibility(\%) = -\left(\frac{F_1 \cdot F_2 \cdot F_3}{60}\right) \cdot 100 \quad (4)$$

The 'Compute Planar KSI' and 'Compute Wedge KSI' functions generate 3D visualizations with discontinuities color-coded according to five susceptibility classes (Fig. 7). The planes susceptible to freefall or sliding without retaining structure contact are assigned distinct colors outside the standard scale to highlight these critical cases.

3.4 Dynamic Analysis

3.4.1 Volume Calculation

The dynamic analysis modules calculate the volume of potentially unstable blocks, needed for calculating gravitational driving forces. The 'Planar Volume Side ½' and 'Wedge Volume' functions partition the point cloud with the following logic (Fig. 8):

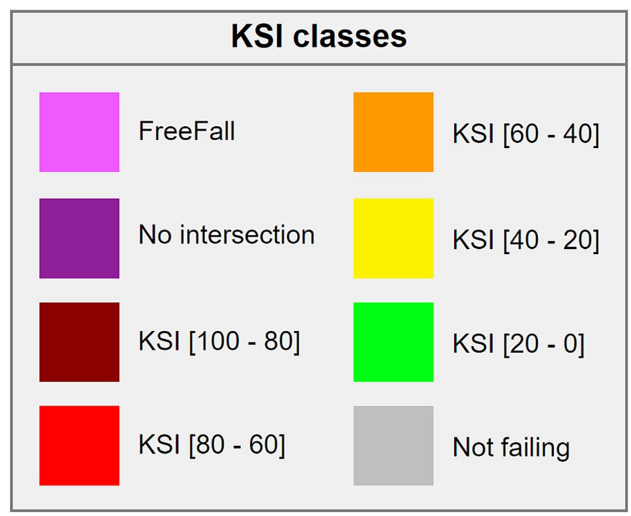

Fig. 7 RoDiAn susceptibility legend of KSI classes

1. For each point in the 3DPC, compute the dot product between the plane's normal vector and the vector from the plane center to the point;
2. Classify points as Side 1 (non-negative dot product) or Side 2 (negative dot product);
3. Generate convex hulls for each partition and calculate enclosed volumes.

The choice of a convex hull representation is primarily driven by topological constraints inherent to point clouds

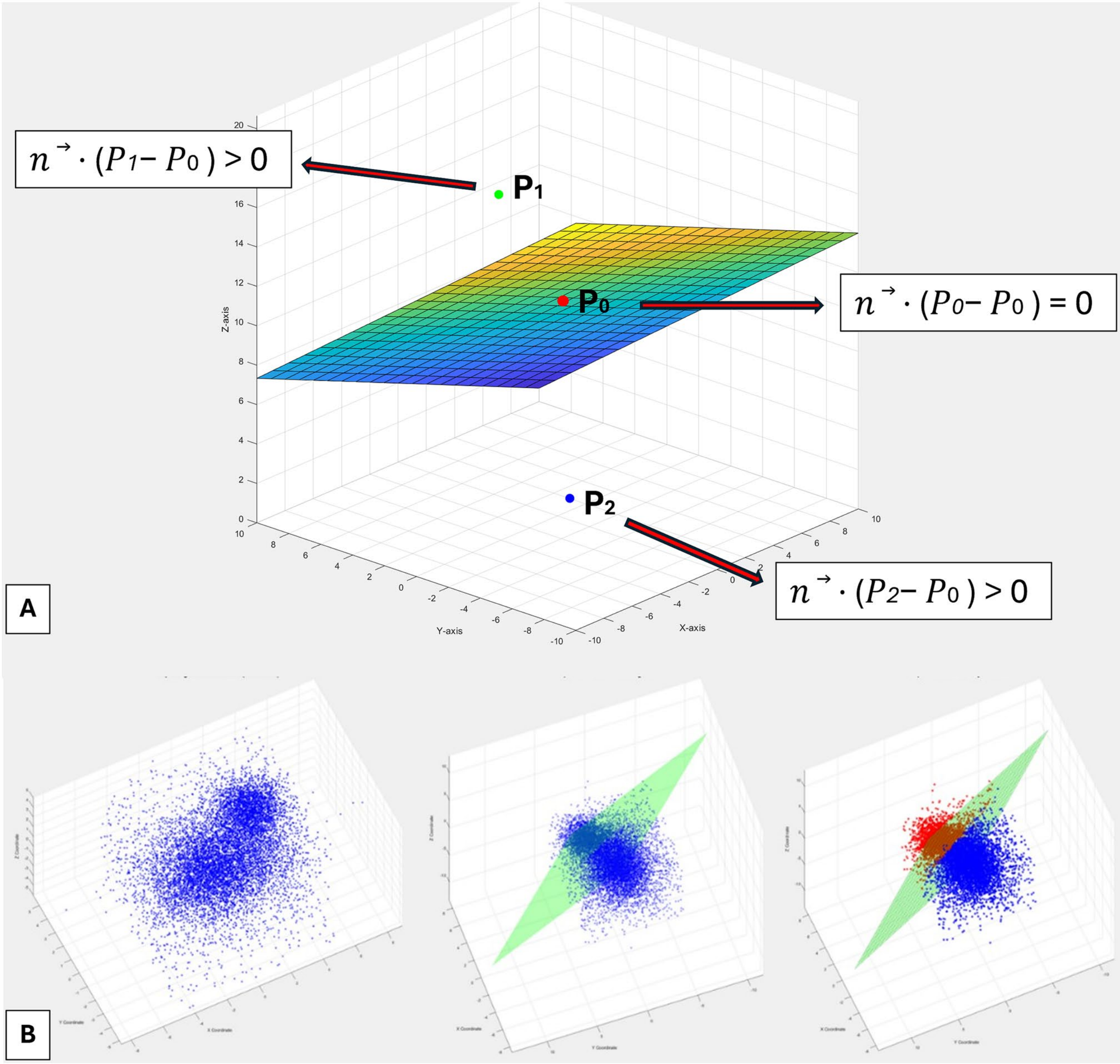

Fig. 8 Illustration of the volume calculation logic in RoDiAn. **A**: The plane separates the point cloud into two sides based on the dot product between the plane's normal vector $\vec{n}$ and the vector from the plane center P_0 to each point P_i. Points with non-negative dot products ($\vec{n} \cdot (P_i - P_0) > 0$) are assigned to Side 1, while points with negative dot products ($\vec{n} \cdot (P_i - P_0) < 0$) are assigned to Side 2. Points lying on the plane satisfy $\vec{n} \cdot (P_i - P_0) = 0$. **B:** Point cloud classification and separation by a discontinuity plane. Left: Original 3DPC (3D Point Cloud). Center: Plane intersecting the point cloud. Right: Separated subclouds with points classified into Side 1 (red) and Side 2 (blue) based on their position relative to the plane

acquired from building facades. Since protruding architectural elements are scanned without a closed rear face, alternative triangulation methods produce unreliable volume estimates due to the inherent concavity introduced by the missing back surface. Users are recommended to inspect the 3D hull visualization against the original point cloud to assess the magnitude of any overestimation for specific blocks exhibiting pronounced concavities.

3.4.2 Sliding Area Calculation

The 'Planar Area' and 'Wedge Area' functions determine the contact area along discontinuity surfaces, required for normal stress calculation in shear strength criteria. The logic is the following:

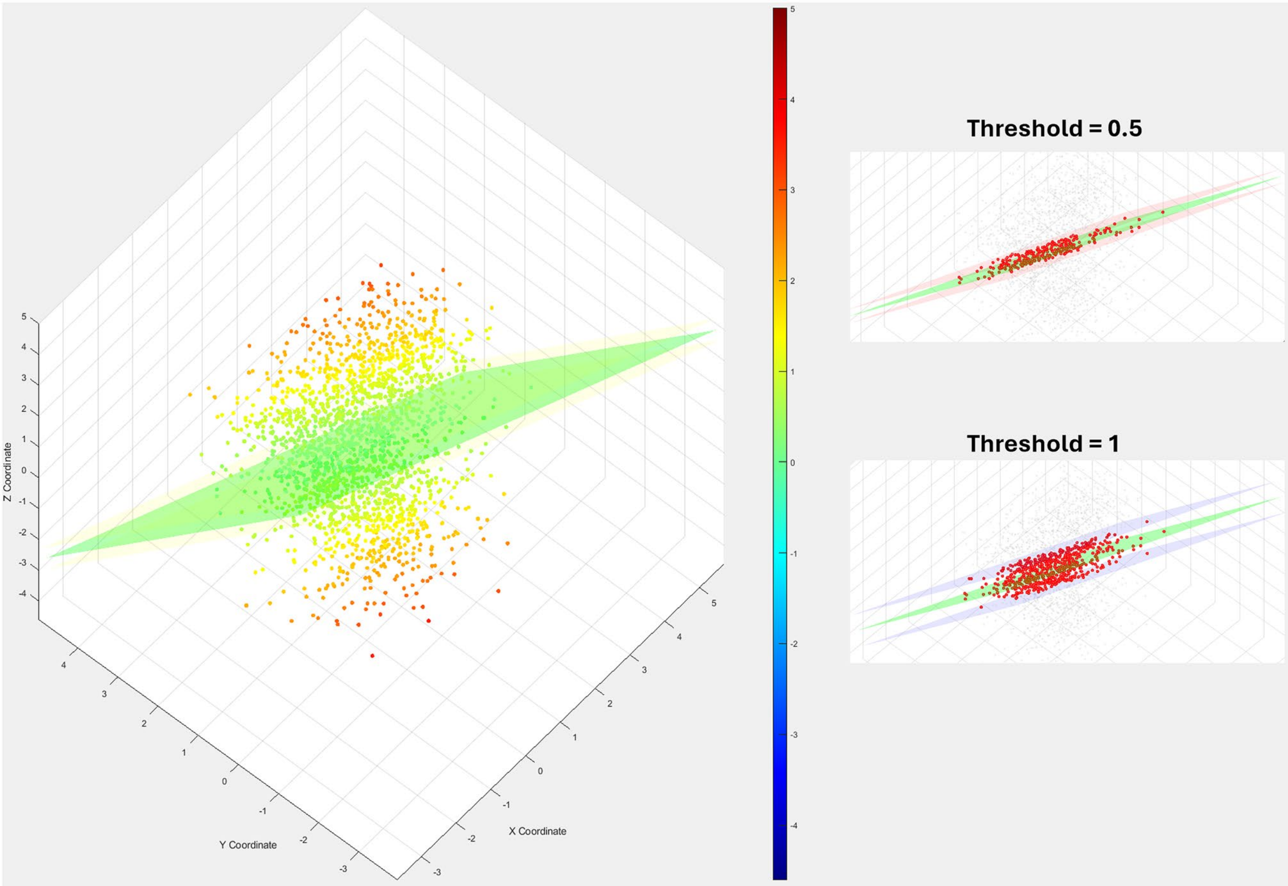

Fig. 9 Threshold-based selection of points belonging to the discontinuity plane. Left: Point cloud colored by distance from the plane. Right: resulting point selections illustrating how different threshold values affect which points are identified as belonging to the plane; a smaller threshold value (top, 0.5) includes less point than an higher one (bottom, 1)

1. Computing the perpendicular distance from each point in the cloud to the selected plane.
2. Applying a user-adjustable threshold to identify points belonging to the discontinuity surface (Fig. 9).
3. Projecting selected points onto a 2D coordinate system within the plane.
4. Computing the convex polygon of the projected points and calculating its area.

The recommended procedure is to begin with a low threshold and progressively increase it while monitoring the 2D convex hull projection (Fig. 10): the threshold should be set at the lowest value at which the projected polygon visually converges to cover the full observable joint trace on the block surface without capturing large numbers of off-plane points from adjacent surfaces. In practice, this corresponds to the value beyond which increasing the threshold adds disproportionately large area increments by incorporating neighboring surface geometry. Because this parameter introduces operator-dependency, users should document the selected threshold value as part of the analysis record to ensure reproducibility. The 2D projection of selected points onto the plane coordinate system, displayed automatically by the software (Fig. 10), provides a meaningful visual check on whether the identified polygon is a plausible representation of the sliding contact zone.

3.4.3 Safety Factor Calculation

The ‘Compute Safety Factor’ functions performs limit equilibrium analysis using the geometrical inputs, the block volume (V) and sliding surface area (A), directly from the spatial analysis presented above. These are then combined with material properties entered by the user to calculate stability according to the selected failure criterion. RoDiAn implements both the Barton–Bandis and Mohr–Coulomb failure criteria. In this section, Barton’s shear strength criterion (Barton 1973) is used as the illustrative example; the choice of criterion should be guided by the available site characterization data and the nature of the discontinuity surfaces. For this specific model, the user defines the relevant rock mass properties through dedicated interactive fields:

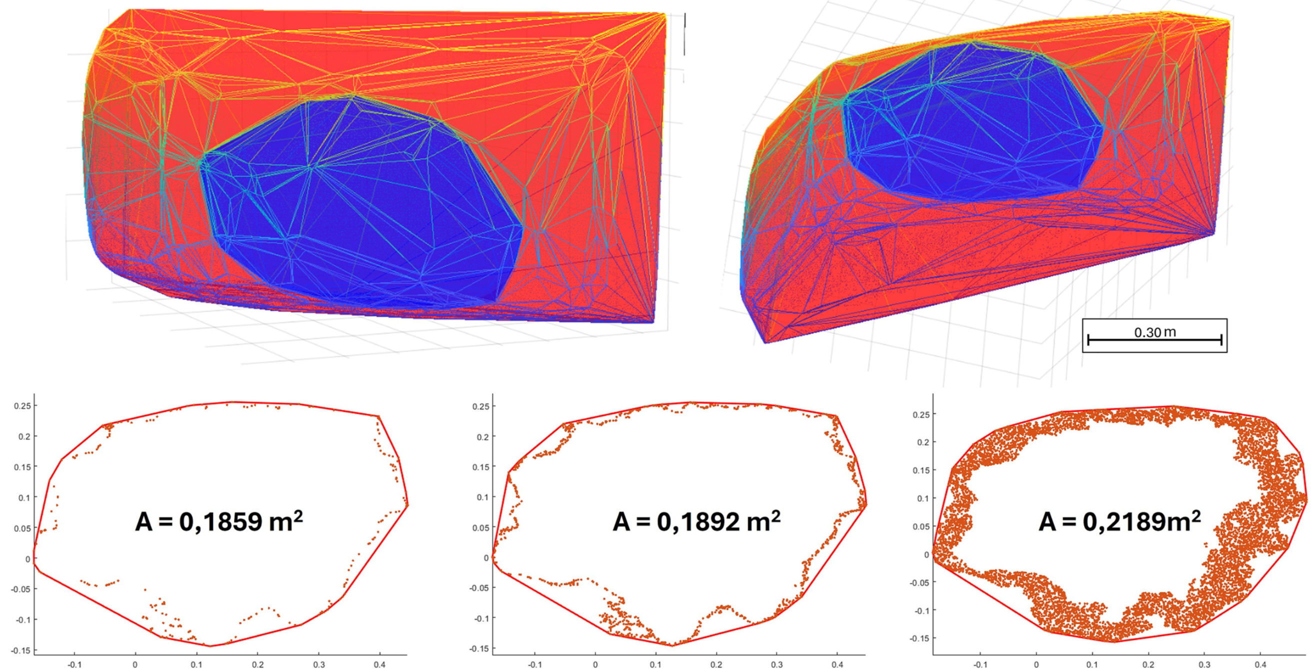

Fig. 10 Convex hull computation and area calculation of the discontinuity plane. Top: 3D visualization showing the sliding area (blue) within the point cloud (red) from two perspectives. Bottom: 2D projections of the convex hull onto the plane with computed areas ranging from 0.1859 m^2 to 0.2189 m^2, demonstrating how the threshold selection affects the calculated sliding contact area. The plotted polygon allows visual validation of whether it reasonably covers the sliding contact region

- Joint roughness coefficient (JRC)
- Residual friction angle (φ)
- Joint Wall Compressive Strength (JCS)
- Rock density (ρ)

For geometrically valid sliding scenarios (non-freefall cases), the software:

1. Calculates normal stress on the sliding surface
2. Applies Barton's criterion
3. Computes resisting force: R
4. Computes driving force: D
5. Determines Factor of Safety: FS = R/D
6. Determines Residual Driving Forces: D—R

The results are displayed in dedicated output fields in the GUI. The residual driving forces are meant to be used for designing stabilization systems, as they quantify the force deficit required to achieve equilibrium. For freefall cases where frictional resistance is absent, the software reports only the residual driving force, which equals the full weight of the potentially detaching block.

4 Results

4.1 Case Study Context

We demonstrate RoDiAn's application through the analysis of rusticated sandstone blocks from the facade of an historical palace in Florence, Italy. The lithotype in example is chosen for its systematic discontinuity networks made of primary bedding planes and calcite veins that allows us to observe a full range of possible cases. Point clouds of individual facade blocks were acquired through close-range photogrammetry and processed using *Agisoft Metashape Pro*. Discontinuities were manually traced in *CloudCompare* and plane parameters exported for RoDiAn analysis. Analysis parameters were set as:

- Facade dip direction: 325°
- Facade dip: 90°
- Friction angle: 25° (Barton and Choubey 1977)
- JRC: 12 (derived from in-situ testing on the failure surfaces)
- JCS: 50 Mpa (derived from in-situ testing with Schmidt Hammer Test)

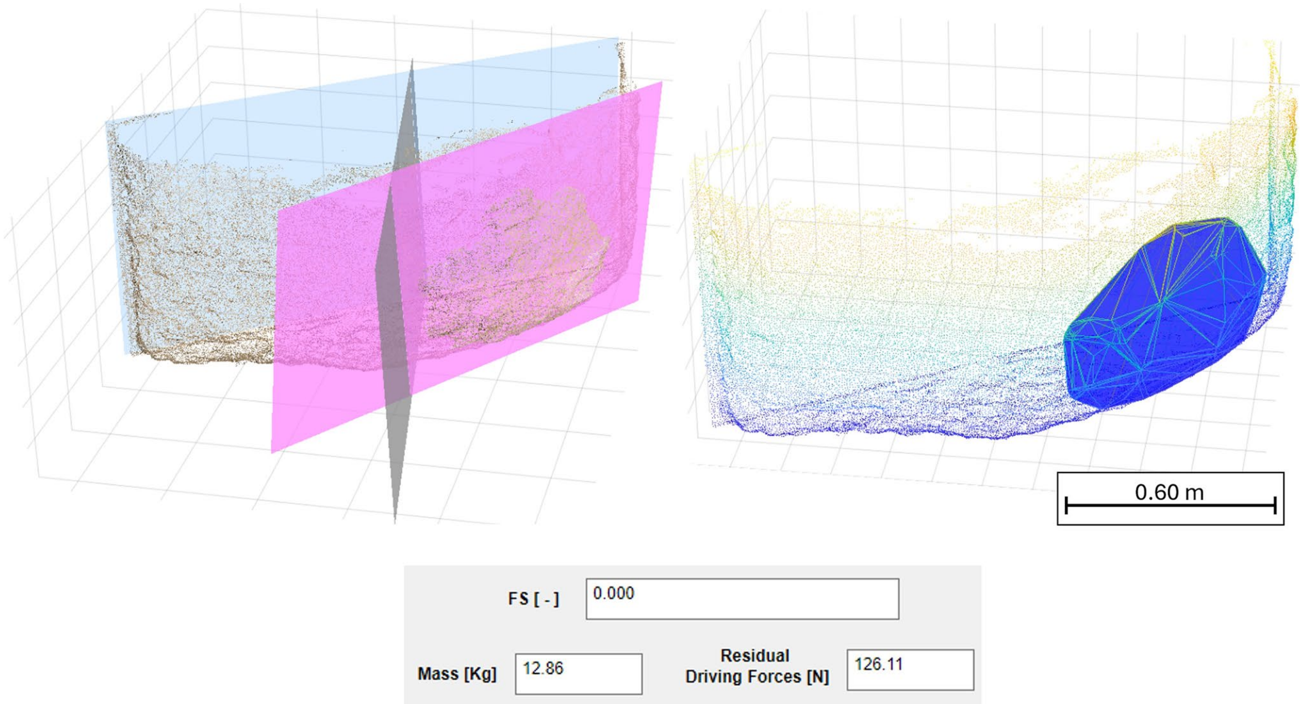

Fig. 11 Block B1. Example of cases with free-fall susceptible discontinuities. Top left: planar susceptibility results; Top right: potentially unstable rock volume; Bottom: dynamic analysis results

- Density: 2700 kg/m.^{3}

4.2 Representative Analysis Cases

4.2.1 Block B1: Single Mechanism

Block B1 (Fig. 11) exemplifies a case where kinematic analysis identifies a single critical mechanism. The block contains multiple discontinuities, but only one plane exhibits geometry susceptible to detachment.

The susceptibility visualization flags this plane in bright purple, distinguishing it from the stable discontinuities shown in gray. Dynamic analysis quantifies the residual driving force at approximately 126.11 N, corresponding to the full weight of the potentially unstable block (mass ≈ 12.86 kg). This value represents a conservative upper bound, as cohesive forces along the discontinuity are not included in the calculation. This information can support engineering decisions regarding stabilization requirements. For example, a fall-arrest device should resist forces exceeding ≈ 130 N to reach equilibrium.

4.2.2 Block B2: Multiple Mechanisms

Block B2 (Fig. 12) demonstrates a more complex scenario where both planar and wedge sliding mechanisms are present. The planar sliding analysis yields a computed safety factor of 0.875 under the assumed input parameters, suggesting that driving forces exceed available frictional resistance for this configuration. The corresponding unstable mass is 18.85 kg, with residual driving forces of 21.99 N. For the identified wedge, the computed safety factor of 1.16 indicates marginally greater resisting than driving forces, with a residual driving force of − 6.66 N (the negative sign indicating a net resisting surplus). These values are presented as indicative outputs whose reliability depends on the accuracy of the input parameters; the dynamic analysis module is intended to demonstrate the tool's computational capability, and site-specific parameter characterization is required before these outputs are used for engineering design decisions.

4.2.3 Block B3: Stable Configuration

Not all analyzed blocks exhibit susceptibility to detachment. Block B3 (Fig. 13) contains multiple visible discontinuities, yet kinematic analysis classifies all as geometrically stable. The susceptibility visualization displays all discontinuities in gray, indicating planes with dip directions approximately perpendicular to the facade (± 90° from favorable sliding orientation) and no wedges intersections in the block.

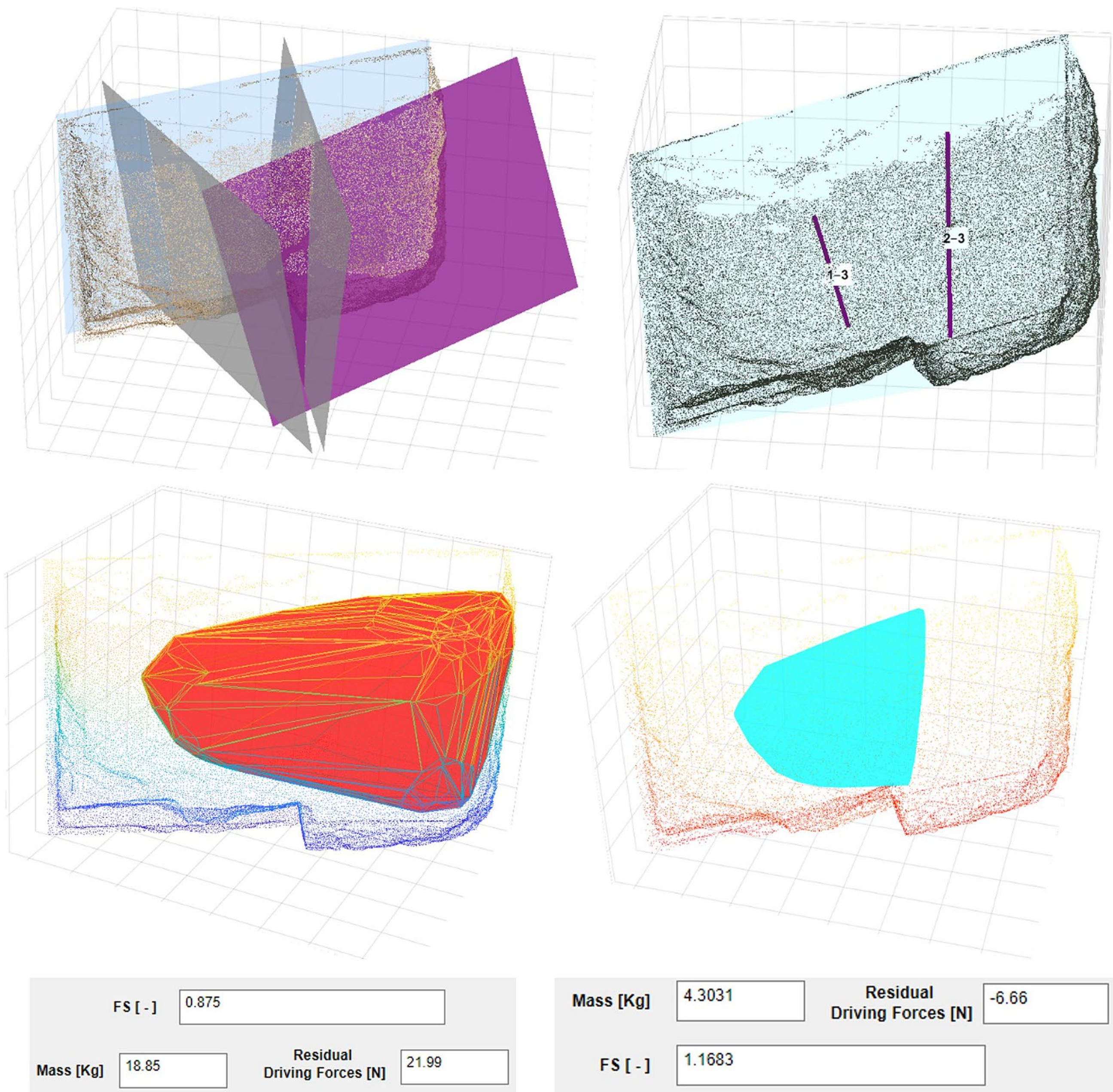

Fig. 12 Block B2. Example of cases with multiple possible kinematic mechanisms. Left: planar susceptibility results and potentially unstable volume; Right: Wedge susceptibility results and potentially unstable volume; Bottom: dynamic analysis results

4.3 Software Validation

RoDiAn has been tested and validated in its computational functions through two distinct approaches:

• Spatial and geometric computation functions were validated using synthetic point clouds with known mathematical properties.

• Kinematic analysis functions were validated using point clouds from a real-world case study, by comparison with one of the industry-standard software tools, *Rocscience Dips*.

It is important to clarify that the functions validated in this section are those involving internal logic beyond the direct application of algebraic formulas from literature. In cases where a function applies a formula directly (e.g., Compute Safety Factor), validation is considered implicit, given the transparency of the code and the explicit formulation of the equations.

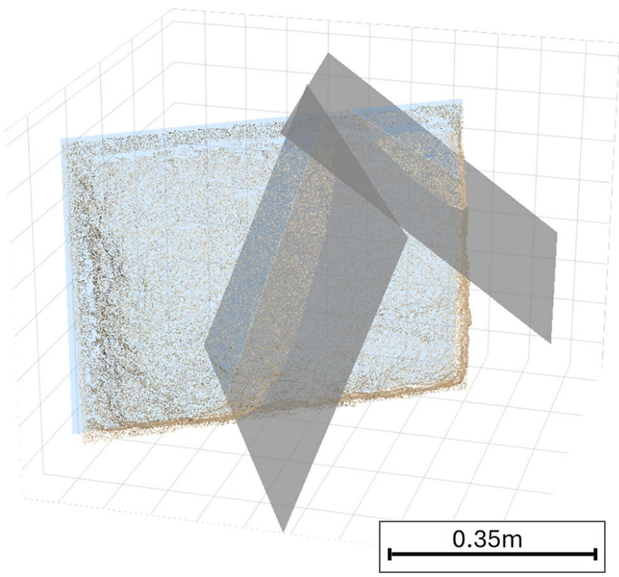

Fig. 13 Block B3. Example of cases with discontinuities oriented in stable configurations

4.3.1 Geometric Validation

Three basic geometries were tested: rectangular parallelepiped (1 × 1 × 2 m), square-based pyramid (1 m base), hemisphere (1 m diameter). Discontinuity planes were applied at various orientations and volumes were calculated using the planar functions (Fig. 14) and then compared against theoretical values. The results (Table 1) demonstrated errors below ≈ 3% in all cases, with discrepancies primarily attributable to point cloud density limitations rather than algorithmic issues.

A similar approach was used to validate the Wedge volume functions, in which the complementary volumes obtained from wedge partitioning (Fig. 15) were calculated and compared with theoretical values. The results (Table 2) revealed low overall errors (below ≈ 5%).

4.3.2 Kinematic Analysis Validation

A sample block (Fig. 16) containing three discontinuities was analyzed using both software packages. RoDiAn correctly identified: one plane susceptible to planar sliding (Plane 3), two wedges susceptible to sliding (Wedges 1–3 and 2–3). In addition to confirming agreement in susceptibility classification, the validation case in Fig. 16 illustrates the spatial filtering capability that distinguishes RoDiAn from conventional stereographic analysis. For the sample block, the three discontinuity planes generate three possible intersection lines (1–2, 1–3, and 2–3). RoDiAn's wedge filtering algorithm evaluates each intersection line against the convex hull of the block point cloud and retains only those that physically occur within the block geometry. Intersection line 1–2 was identified as lying outside the block boundaries and was therefore excluded from the kinematic analysis as a non-physical wedge.

The validation was extended to 49 blocks, consistently showing agreement in kinematic classification and wedge filtering capabilities.

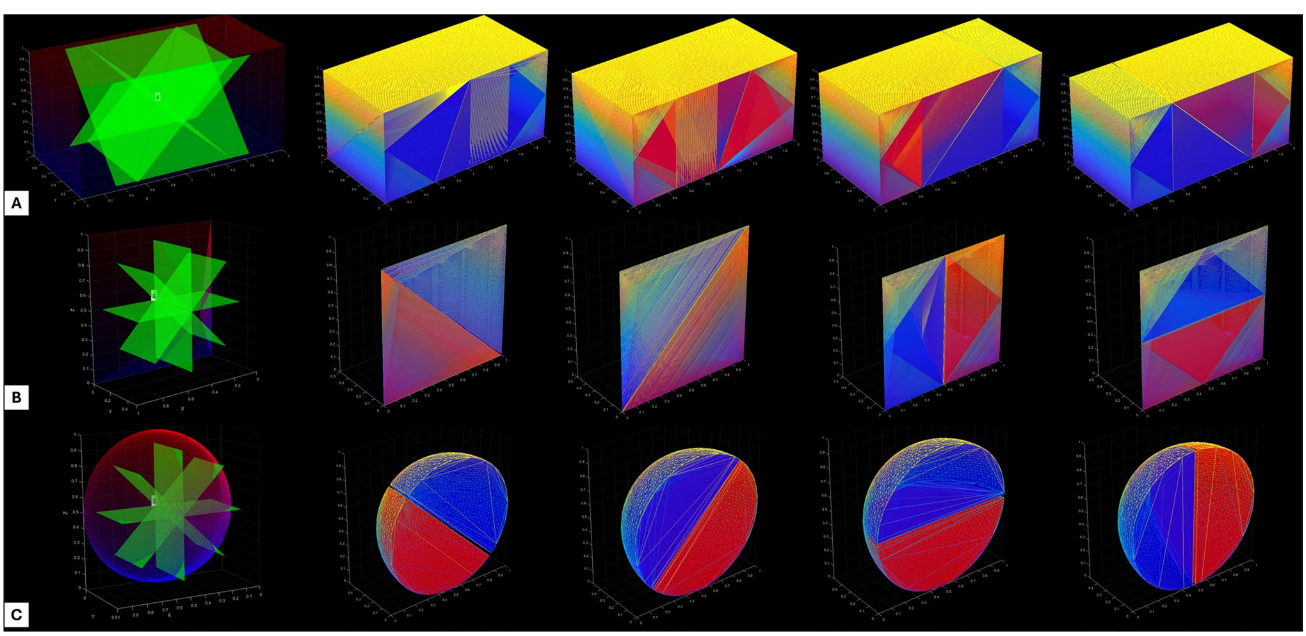

Fig. 14 Validation of Planar volume calculation functions on the synthetic point clouds. **A:** Parallelepiped. **B**: Pyramid. **C**: Hemisphere

Table 1 Comparison of measured (Tot V) and reference volumes (Tot V (ref.)) for the parallelepiped (Para), pyramid (Pyra) and hemisphere (Hemi) point cloud using the Planar volume function

Plane	V Side 1	V Side 2	Tot V	Tot V (ref.)	Error (%)
Para-1	0.9950	0.9950	1.990	2.000	0.50
Para-2	0.9950	0.9950	1.990	2.000	0.50
Para-3	0.9975	0.9975	1.995	2.000	0.25
Para-4	0.9975	0.9975	1.995	2.000	0.25
Pyra-1	0.0896	0.8799	0.9695	1.000	3.05
Pyra-2	0.0896	0.8799	0.9695	1.000	3.05
Pyra-3	0.0839	0.8890	0.9729	1.000	2.71
Pyra-4	0.0839	0.8890	0.9729	1.000	2.71
Hemi-1	0.1307	0.1243	0.2550	0.2615	2.49
Hemi-2	0.1262	0.1302	0.2564	0.2615	1.95
Hemi-3	0.1303	0.1261	0.2564	0.2615	1.95
Hemi-4	0.1230	0.1302	0.2532	0.2615	3.17

5 Discussion and Conclusions

This work presents a new methodological framework and its associated software implementation for quantifying rockfall susceptibility in masonry and engineered rock structures. This methodology adapts parameters and conceptual criteria originally developed for the kinematic and dynamic analysis of natural rock masses. This is both an intentional and a necessary choice, given the current absence of any quantitative framework specifically designed for block-scale gravitational instability in architectural contexts. As a deliberate conceptual choice, the software modifies as few elements as possible from classical kinematic and dynamic analysis, so that the geomechanical expertise and measurement protocols accumulated over decades of practice remain directly applicable, and the aspects requiring independent validation are limited to the geometric functions, which have been validated in this work.

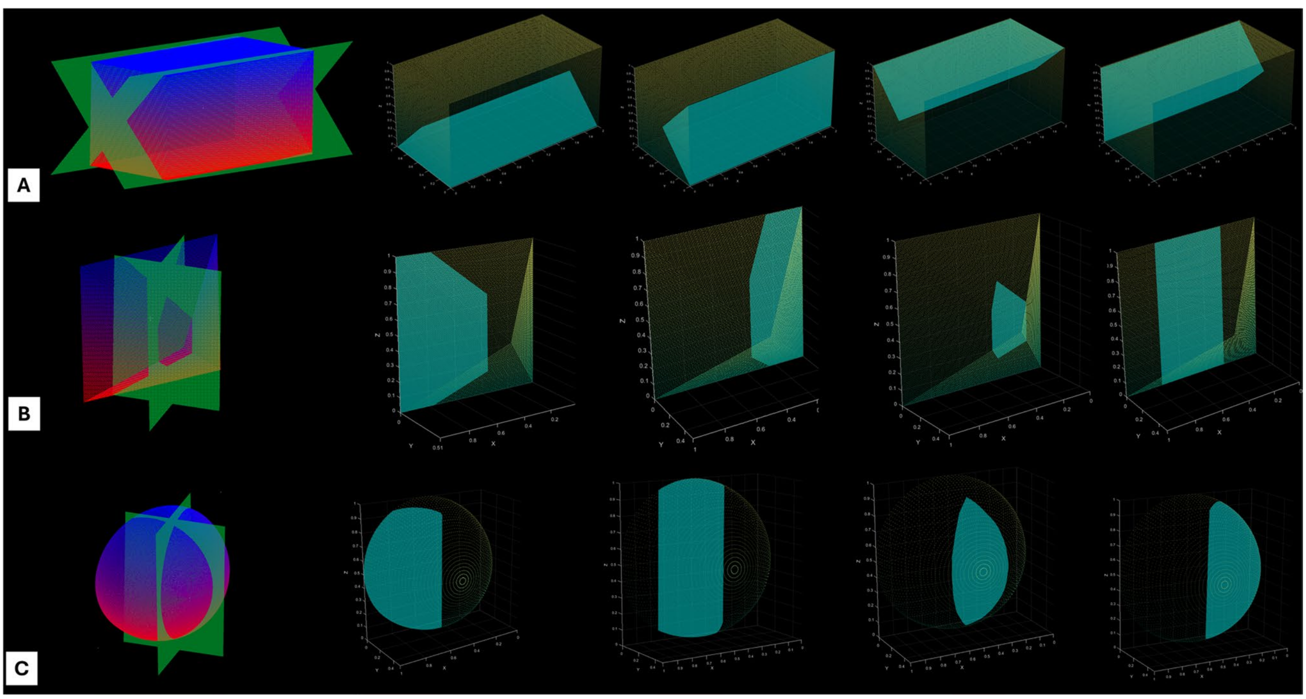

Fig. 15 Validation of Wedge volume calculation functions on the synthetic point clouds. **A:** Parallelepiped. **B**: Pyramid. **C:** Hemisphere

Table 2 Comparison of measured (Tot V) and reference volumes (Tot V (ref.)) for the parallelepiped, pyramid and hemisphere point cloud using the Wedge volume function

ID	V_1	V_2	V_3	V_4	Tot V	Tot V (ref.)	Error (%)
Parallelepiped	0.4886	0.4886	0.4886	0.4886	1.9544	2.0000	2.28
Pyramid	0.0069	0.0510	0.0484	0.0510	0.1573	0.1666	5.58
Hemisphere	0.0274	0.0868	0.0594	0.0868	0.2604	0.2618	0.53

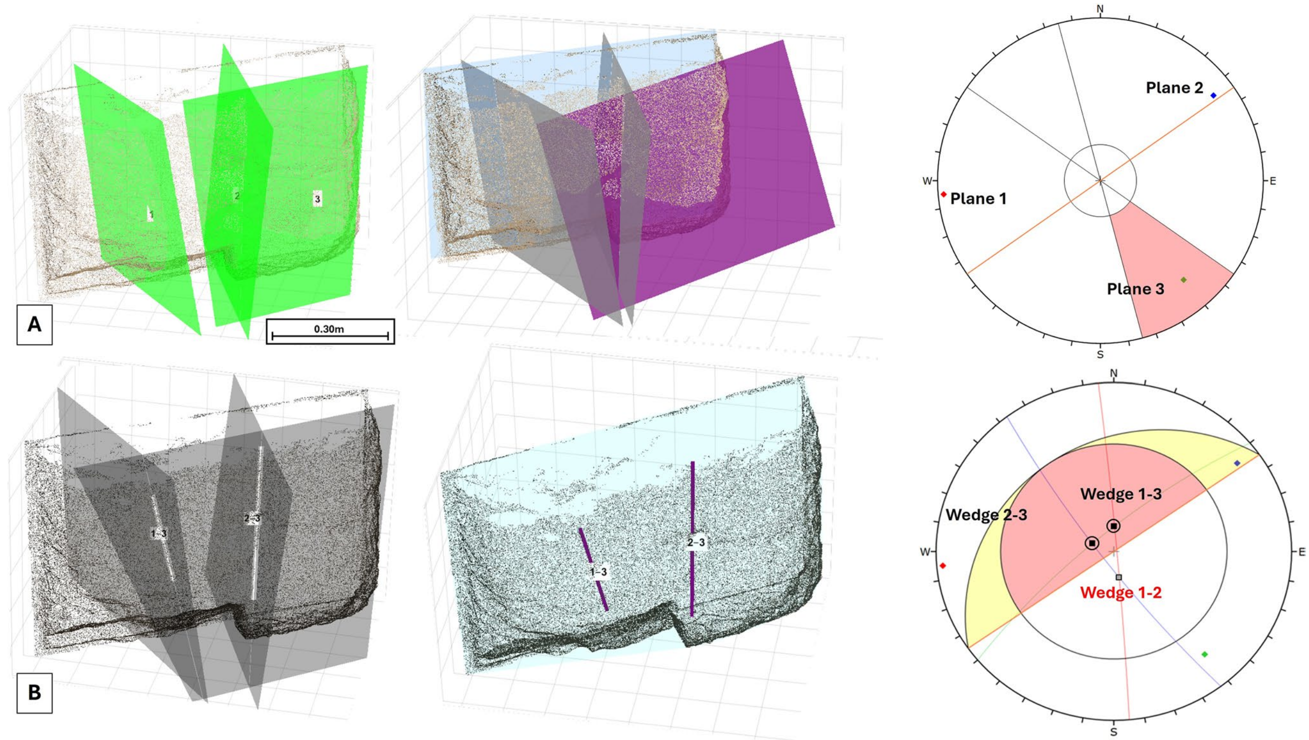

Fig. 16 **A:** RoDiAn (left) and RocScience Dips (right) planar sliding Kinematic analysis results for the sample block. **B:** RoDiAn (left) and RocScience Dips (right) wedge sliding Kinematic analysis results for the example block: the wedges formed within the block (1–3 and 2–3) are highlighted in black. The 1–2 wedge, highlighted in red, does not develop within the block and is automatically excluded by Rodian

Nonetheless, several important distinctions between the geological and architectural domains must be acknowledged. At the scale of individual blocks, the large-scale assumptions applicable to natural rock masses (e.g., geological correlation of joint properties across the slope, infinite discontinuity persistence, and statistically meaningful family distributions) cannot be applied, since each block has been individually quarried, shaped, and repositioned. The scale of analysis is therefore necessarily that of the single block, within which the mechanical properties and frictional behavior of discontinuities remain consistent with those observed in natural settings. For this reason, only concepts whose validity remains applicable at this scale of observation have been adopted. The Kinematic Susceptibility Index derived from the SMR adjustment factors F1–F2–F3 retains its physical meaning as a geometric susceptibility indicator at the block scale: the same angular relationships between discontinuity orientation, free face, and friction angle that govern kinematic feasibility on natural slopes apply equally to discrete blocks. Likewise, the principles of dynamic analysis remain applicable at this scale, since the failure criteria employed (Barton–Bandis and Mohr–Coulomb) were originally developed to model discontinuity-controlled detachments of dimensions comparable to those observable in both natural and architectural settings.

Given that the fundamental principle of the methodology is the application of concepts derived from natural rock masses, the methodology does not apply to artificial blocks, cemented masonry systems, or elements for which no protrusion from the wall surface exists, since a flat surface does not provide sufficient geometric information to reconstruct the three-dimensional orientation of internal discontinuities. For blocks integrated into a cemented masonry system, the facade interaction test is nonetheless useful for identifying elements that are in contact with a backing structure capable of providing additional resistance beyond that captured by the limit equilibrium model.

Several other limitations in the current implementation require consideration. The safety factor outputs produced by RoDiAn should be interpreted as indicative screening values rather than as definitive stability numbers. The Barton-Bandis input parameters (JRC, JCS, and φr) each carry inherent measurement or estimation uncertainty that propagate directly into the computed FS. Sensitivity analysis, varying input parameters across their plausible ranges, is recommended before FS values are used as the basis for engineering design decisions. The computed FS should therefore be treated as a relative ranking metric for prioritizing inspection and intervention, not as a certified engineering reliability estimate. Both the Barton-Bandis and Mohr–Coulomb criteria are available in RoDiAn, and Mohr–Coulomb parameters (cohesion and friction angle) may be more appropriate where mortar or discontinuity infill material contributes to joint resistance.

The current workflow requires manual tracing and plane fitting in CloudCompare and represents the most time-intensive component of the analysis. For a facade containing hundreds of blocks, the cumulative time investment may be substantial, and this practical constraint should be factored into the planning of any large-scale assessment campaign. Manual tracing also introduces subjective elements into an otherwise quantitative methodology. While automated discontinuity detection would partially address these issues, its application to man-made architectural elements faces several obstacles. Traditional scanline and automated clustering algorithms designed for natural rock masses rely on morphological signatures such as planar joint sets with consistent orientation statistics, features that do not exist in carved and sculpted architectural elements where surfaces have been intentionally modified. Man-made structures also present extreme feature heterogeneity: the features of interest range from geological veins and bedding planes to hairline cracks and structural fractures that may be morphologically indistinguishable from decorative carvings and tooling marks. For large facades composed of similarly dressed stone blocks with consistent surface treatments, semi-automated discontinuity detection may prove effective and could be explored as a future development. However, such approaches cannot be generalized across the full spectrum of architectural contexts and require case-by-case evaluation of their applicability. Interpretation of results for conservation practice

The recommended workflow for applying RoDiAn results in a conservation context is as follows. The kinematic screening step (Sect. 3.3) provides a conservative first-pass estimate of which blocks are geometrically capable of detaching. This step is conservative by design: blocks classified as kinematically unstable may in practice be stabilized by cohesive forces, interlocking, or mortar that the model does not account for. Among blocks identified as kinematically susceptible, the KSI provides a relative ranking of geometric unfavourability to prioritize which blocks warrant further investigation. The dynamic analysis module (Sect. 3.4) can then be applied to the highest-priority blocks to quantify the margin between driving and resisting forces under the assumed input parameters. For the least stable blocks, particularly those with computed FS below 1.0 or with large residual driving forces, strategies can be defined for either targeted in-situ investigation to refine input parameters or direct safety intervention such as the installation of fall-arrest nets or anchoring systems, using the residual driving force output to size the restraint.

No prescriptive hazard thresholds or numerical FS cutoff values are defined in this work, as these decisions are context-dependent and governed by factors including acceptable risk level, the presence of the public, economic feasibility of intervention, and the conservation constraints of the specific building. These judgements require case-by-case expert assessment. The role of RoDiAn is to provide quantitative geometric susceptibility, kinematic classification, and force balance to make such judgements informed and reproducible.

Acknowledgements The authors gratefully acknowledge Francesco Di Meo for his contributions through his thesis work "Stability analysis methods on stone portions of architectural cultural heritage" which supported the development of this methodology.

Author contributions Eugenio Segabinazzi: conceptualization, methodology, software, formal analysis, writing—original draft. Teresa Salvatici: conceptualization, methodology, writing—review and editing. Giovanni Gigli: conceptualization, writing—review and editing. Adrián J. Riquelme: conceptualization, writing—review and editing. Emanuele Intrieri: conceptualization, methodology, writing—review and editing, supervision, project administration.

Funding Open access funding provided by Università degli Studi di Firenze within the CRUI-CARE Agreement. This research received no external funding

Code and data availability Name of the code/library: RoDiAn. Contact: eugenio.segabinazzi@unifi.it. Program language: MATLAB. Software required: MATLAB R2023b and MATLAB Runtime R2023b. Program size: 3.42 MB (MATLAB app) 5.75 MB (Windows installer). RoDiAn software, installation instructions, and test datasets are available at: https://github.com/eugeniosegabinazzi-DST-UNIFI/RoDiAn

Declarations

Conflict of interest The authors declare that they have no known competing financial interests or personal relationships that could have appeared to influence the work reported in this paper.

References

Azarafza M, Akgün H, Ghazifard A, Asghari-Kaljahi E, Rahnamarad J, Derakhshani R (2021) Discontinuous rock slope stability analysis by limit equilibrium approaches – a review. Int J Digit Earth 14:1918–1941. https://doi.org/10.1080/17538947.2021.1988163

Barton N (1973) Review of a new shear-strength criterion for rock joints. Eng Geol 7:287–332. https://doi.org/10.1016/0013-7952(73)90013-6

Barton N, Choubey V (1977) The shear strength of rock joints in theory and practice. Rock Mech Rock Eng 10:1–54. https://doi.org/10.1007/BF01261801

Chang W, Xing A, Zhang Y (2024) Dynamic fragmentation characteristics of a heavily jointed rock avalanche: DEM simulation and field seismic signal analysis. Comput Geotech 172:106459. https://doi.org/10.1016/j.compgeo.2024.106459

Dorren LKA (2003) A review of rockfall mechanics and modelling approaches. Prog Phys Geogr Earth Environ 27:69–87. https://doi.org/10.1191/0309133303pp359ra

Gigli G, Casagli N (2011) Semi-automatic extraction of rock mass structural data from high resolution LIDAR point clouds. Int J Rock Mech Min Sci 48:187–198. https://doi.org/10.1016/j.ijrmms.2010.11.009

Gigli G, Lombardi L, Carlà T, Beni T, Casagli N (2022) A method for full three-dimensional kinematic analysis of steep rock walls based on high-resolution point cloud data. Int J Rock Mech Min Sci 157:105178. https://doi.org/10.1016/j.ijrmms.2022.105178

Gurrieri F. (Eds) (2009). La città a pezzi, pezzi di città: distacchi lapidei a Firenze; 1977 - 2009, DIRES / Quaderni della fototeca. Ed. Polistampa, Firenze.

Hantz D, Corominas J, Crosta GB, Jaboyedoff M (2021) Definitions and concepts for quantitative rockfall hazard and risk analysis. Geosciences (Basel) 11:158. https://doi.org/10.3390/geosciences11040158

Hudson JA, Harrison JP (2007) Engineering rock mechanics: an introduction to the principles, Repr. ed. Pergamon, Oxford

Itasca Consulting Group, Inc. (2019) UDEC - Universal distinct element code, Ver. 7.0. Minneapolis: Itasca.

Itasca Consulting Group, Inc. (2024) 3DEC - Three-dimensional distinct element code, Ver. 9.0. Minneapolis: Itasca.

Jaiswal A, Verma AK, Singh TN (2024) A critical review of rock mass classification systems for assessing the stability condition of rock slopes. Environ Earth Sci 83:245. https://doi.org/10.1007/s12665-024-11532-2

Jiang S-H, Chen J-D, Wang ZZ, Zheng J, Huang J, Lü Q (2024) Three-dimensional discrete element analysis of jointed rock slope stability based on the universal elliptical disc model. Rock Mech Rock Eng 57:505–525. https://doi.org/10.1007/s00603-023-03575-x

Kundu J, Sarkar K, Verma AK, Singh TN (2022) Novel methods for quantitative analysis of kinematic stability and slope mass rating in jointed rock slopes with the aid of a new computer application. Bull Eng Geol Environ 81:29. https://doi.org/10.1007/s10064-021-02524-8

Menegoni N, Giordan D, Perotti C (2021) An open-source algorithm for 3D rock slope kinematic analysis (ROKA). Appl Sci 11:1698. https://doi.org/10.3390/app11041698

Menegoni N, Giordan D, Inama R, Perotti C (2023) DICE: an open-source MATLAB application for quantification and parametrization of digital outcrop model-based fracture datasets. J Rock Mech Geotech Eng 15:1090–1110. https://doi.org/10.1016/j.jrmge.2022.09.011

Palamidessi A, Segabinazzi E, Calandra S, Centauro I, Salvatici T, Garzonio CA, Intrieri E (2026) Monument rockfall risk assessment: a systematic approach to risk classification in cultural heritage sites. Heritage 9(3):122. https://doi.org/10.3390/heritage9030122

Pantelidis L (2009) Rock slope stability assessment through rock mass classification systems. Int J Rock Mech Min Sci 46:315–325. https://doi.org/10.1016/j.ijrmms.2008.06.003

Pastor JL, Riquelme AJ, Tomás R, Cano M (2019) Clarification of the slope mass rating parameters assisted by SMRTool, an open-source software. Bull Eng Geol Environ 78:6131–6142. https://doi.org/10.1007/s10064-019-01528-9

Riquelme AJ, Abellán A, Tomás R, Jaboyedoff M (2014) A new approach for semi-automatic rock mass joints recognition from 3D point clouds. Comput Geosci 68:38–52. https://doi.org/10.1016/j.cageo.2014.03.014

Romana MR (1993) A geomechanical classification for slopes: slope mass rating. Rock testing and site characterization. Elsevier, pp 575–600. https://doi.org/10.1016/B978-0-08-042066-0.50029-X

Romana M., Tomás R., Serón J.B (2015). Slope MASS Rating (SMR) geomechanics classification: thirty years review. Presented at the 13th ISRM International Congress of Rock Mechanics, p. ISRM-13CONGRESS-2015–131.

Salvatici T, Centauro I, Calandra S, Segabinazzi E, Intrieri E, Garzonio CA (2023) Non-destructive methods applied for in situ mechanical diagnosis: florentine historical buildings in Pietra Serena. Herit Sci 11:116. https://doi.org/10.1186/s40494-023-00959-8

Schiavoni M, Roscini F, Clementi F (2025) Comparative analysis between continuous and discontinuous methods for the assessment of a cultural heritage structure. Meccanica 60:1957–1982. https://doi.org/10.1007/s11012-024-01885-0

Segabinazzi E., Salvatici T., Centauro I., Intrieri E., Calandra S., Garzonio C.A (2024). Applying a geomechanical approach to mitigate rockfall risk from stone heritage buildings, In: New Challenges in Rock Mechanics and Rock Engineering. Presented at the EuRock 2024, Taylor Francis, p. 6. https://doi.org/10.1201/9781003429234

Segabinazzi E, Centauro I, Salvatici T, Calandra S, Intrieri E, Garzonio CA (2026) Architectural heritage monitoring: implementing data-driven preservation for stone corbels with low-code app tools and reporting. In: Furferi R, Governi L, Volpe Y, Gherardini F, Seymour K (eds) The future of heritage science and technologies II. Springer Nature Switzerland, Cham, pp 355–368. https://doi.org/10.1007/978-3-031-98379-5_27

Siddique T (2024) Rock mass classification in slope engineering with special emphasis on Slope mass rating: current status and future projections. Geol J 59:2472–2486. https://doi.org/10.1002/gj.4933

Thiele ST, Grose L, Samsu A, Micklethwaite S, Vollgger SA, Cruden AR (2017) Rapid, semi-automatic fracture and contact mapping for point clouds, images and geophysical data. Solid Earth 8:1241–1253. https://doi.org/10.5194/se-8-1241-2017

Tomás R, Delgado J, Serón JB (2007) Modification of slope mass rating (SMR) by continuous functions. Int J Rock Mech Min Sci 44:1062–1069. https://doi.org/10.1016/j.ijrmms.2007.02.004

Wang Q, Xing A, Xu X, Zhou Y, Yang Q, Song H, Peng J, Zhai L, Bilal M, Liu Y (2024) Formation mechanism and dynamic process of open-pit coal mine landslides: a case study of the Xinjing landslide in Inner Mongolia, China. Landslides 21:541–556. https://doi.org/10.1007/s10346-023-02193-6

Wylie DC, Mah CW (2004) Rock slope engineering: civil and mining, 4th ed. Spon Press, New York